AIP | Journal of Applied Physics

# Optimization of ultra-soft CoZrTa/SiO2/CoZrTa trilayer elements for integrated inductor structures

Cheng Cheng, Ryan Davies, Noah Sturcken, Kenneth Shepard, and William E. Bailey

Citation: J. Appl. Phys. **113**, 17A343 (2013); doi: 10.1063/1.4801524
View online: http://dx.doi.org/10.1063/1.4801524
View Table of Contents: http://jap.aip.org/resource/1/JAPIAU/v113/i17
Published by the American Institute of Physics.

# Optimization of ultra-soft CoZrTa/$SiO_2$/CoZrTa trilayer elements for integrated inductor structures

Cheng Cheng,[1,a)] Ryan Davies,[2] Noah Sturcken,[2] Kenneth Shepard,[2] and William E. Bailey[1]
[1]*Materials Science and Engineering Program, Department of Applied Physics and Applied Mathematics, Columbia University, New York, New York 10027, USA*
[2]*Department of Electrical Engineering, Columbia University, New York, New York 10027, USA*

(Presented 15 January 2013; received 5 November 2012; accepted 7 February 2013; published online 12 April 2013)

We show the optimization of magnetic properties of ferromagnetic (FM)/$SiO_2$/FM trilayer structures as potential candidates for the magnetic core in toroidal integrated inductors, with FM materials $Co_{91.5}Zr_{4.0}Ta_{4.5}$ (CZT) and $Ni_{80}Fe_{20}$ (Py). In the single-layer parent films, we found a monotonic reduction of easy-axis coercivity ($H_c$ down to 0.17 Oe in CZT, 0.4 Oe in Py) with increasing dc magnetron sputtering voltage. In the trilayer rectangular structures, with induced easy-axis in the short lateral dimension, we found proof of dipolar coupling between the two FM layers from BH loop measurements in the CZT system, showing linear response with minimal hysteresis loss when the external field is applied in the long axis. Py elements did not show this optimized property. Further investigation of domain configurations using scanning transmission x-ray microscopy suggests an insufficient induced anisotropy in Py compared with the shape anisotropy to realize the antiparallel-coupled state. © *2013 AIP Publishing LLC* [http://dx.doi.org/10.1063/1.4801524]

Integrated ferromagnetic (FM)-core inductors have been limited in the enhancement of inductance density over air-core structures,[1] due to magnetostatic edge effects. Toroidal, flux-closed structures avoid this problem and can increase the effective permeability to as high as $\mu_r$ of the core.[2] The challenge lies in two aspects. One is engineering an isotropic core, keeping high permeability with low hysteresis loss throughout the closed magnetic flux path, while FM films typically have uniaxial anisotropy.[3] Another is aligning the magnetization transverse to the flux path for high permeability, overcoming the demagnetizing effect from the path shape. $Ni_{80}Fe_{20}$ (Py) ($4\pi M_s = 10.75$ kG, $\rho = 20\,\Omega\cdot$cm) and $Co_{91.5}Zr_{4.0}Ta_{4.5}$ (CZT) ($4\pi M_s = 17$ kG, $\rho = 100\,\Omega\cdot$cm) are well-investigated soft magnetic materials with much application in magnetoelectronics.[4] We choose them as candidates for the toroidal core material and address the above-mentioned two issues accordingly.

First, to achieve isotropy in magnetic films, we use the concept of isotropic high permeability multilayers, proposed by Frommberger *et al.*[5] In an improvement over this prior work, we have incorporated a quadrupole electromagnet into the UHV magnetron sputtering chamber, which enables an *in situ* magnetic field rotating synchronously with the substrate at arbitrary phase difference.[6] Successive laminations of FM material with anisotropy axes rotating at designated step could be obtained in one deposition, without breaking vacuum. In addition, very low Ar pressure during dc sputtering is used in our system, allowing for a mean free path comparable with the target-substrate separation. We show in this paper control of the soft magnetic properties of single-layer extended films by varying the sputtering voltage and thus the kinetic energy of the incident particles, optimizing the building blocks for isotropic multi-layered films.

Second, to arrange the high-permeability axis along the flux path, we fabricate elongated structures (rectangles and stripes) and induce the easy axis (EA) transverse to the long lateral dimension. By using FM/nonmagnetic (NM)/FM trilayers, we expect to produce the easy-axis state in the element originating from the dipolar coupling between the two FM layers.[7] The elimination of domain walls (DWs) (inevitable in the closure-domain states in single-layer patterned elements) leads to nearly pure rotational hard-axis (HA) response when an external field is applied along the elongated direction. We found CZT more suitable for this application with its relatively high induced anisotropy overcoming the shape anisotropy. Negligible hysteresis loss could be achieved in these elements. However, we did not find proof of the easy-axis state in the Py trilayer elements, conflicting with the calculated phase diagrams in Ref. 7.

The power dissipation in metallic inductor cores comes from two sources of loss: eddy currents and hysteresis.[4] Laminating the magnetic alloy film with a dielectric, NM material ($SiO_2$) is thought to inhibit the eddy currents and reduces the coercivity significantly.[8,9] In optimizing the multilayered structure, the first step is to determine the optimal single FM layer thickness $t_{FM}$ and its deposition conditions. To eliminate the eddy currents, $t_{FM}$ should be thinner than the skin depth $\delta$ of the FM material, $\delta_{Py} = 159$ nm, $\delta_{CZT} = 622$ nm at 500 MHz, calculated from the parameters given in Ref. 4. In terms of the hysteresis, we attribute the EA coercivity $H_c^{EA}$ dominantly to the interaction of 180° DWs with surface irregularities, since Py (polycrystalline) and CZT (amorphous) both have zero magnetostriction.[10]

a)Author to whom correspondence should be addressed. Electronic mail: cc3043@columbia.edu

 

The coercive field can be estimated proportional to $\Delta t_{FM}/t_{FM}$, where $\Delta t_{FM}$ is the fluctuation in film thickness. HA coercivity comes from the small local fluctuation of induced anisotropy which leads to ripple domains.[11] The magnetization orienting in the HA in the DWs contributes to the remanent magnetization in HA loop. $H_c^{HA}$ is thus not associated with DW motion. However, longer wavelength of anisotropy dispersion or better film homogeneity will reduce the DW density in the HA remanent state, leading to a reduction in $H_c^{HA}$.

Fig. 1 shows the thickness dependence of EA and HA coercivities in extended single-layer films. The uniaxial anisotropy ($H_k^{Py} = 3.5$ Oe, $H_k^{CZT} = 20$ Oe measured with BH loop tracer) is induced during deposition, by a field of ~75 Oe imposed by the quadrupole electromagnet. The dc sputtering voltage and Ar pressure for Py and CZT were 480 V, 1.3 mTorr and 420 V, 1.2 mTorr, respectively. While thicker amorphous CZT films, up to 500 nm, might have given much lower coercivity (0.015 Oe),[12] we found crystallization in our 400 nm film, confirmed by XRD, leading to an abrupt increase in $H_c$. Elevated substrate temperature during long deposition may contribute to this result since the sample stage is not water-cooled in our system. 100 nm Py film is in the vicinity of transition from cross-tie walls to asymmetric Bloch walls,[13] showing an increase in $H_c^{EA}$, while $H_c^{HA}$ remained at the same level. If we plot the EA coercivity as a function of $1/t_{FM}$ in the region where no DW-type transition or crystallization occurs, the data show linearity, which is expected from $H_c^{EA} \propto \Delta t_{FM}/t_{FM}$. The offset might reflect the intrinsic $H_c$ not associated with the surface property.

Next, we chose the film thicknesses with the lowest coercivity, i.e., 80 nm for Py and 200 nm for CZT, for further optimization in deposition conditions. We keep the lowest possible Ar pressure (~1.2 mTorr) during sputtering for all depositions, with an estimated mean free path of 4 cm, which is comparable with the target-substrate separation of 10 cm.

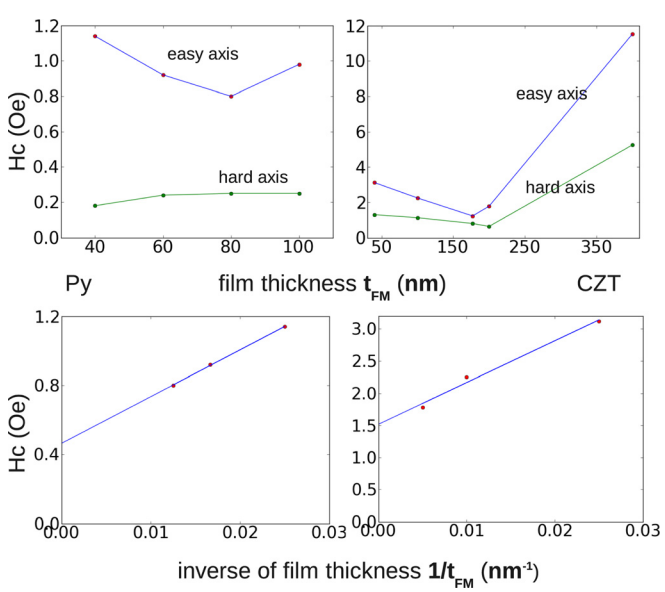


FIG. 1. Thickness ($t_{FM}$) dependence of coercivity ($H_c$) in uniaxial anisotropy extended single-layer films, Py (left) and CZT (right). Lower panel demonstrates the linear dependence of $H_c^{EA}$ on the inverse of $t_{FM}$, $1/t_{FM}$, while $\Delta t_{FM}$ remains at the same level at a specific sputtering voltage.

Sufficient presputtering ensures the target composition in the deposited films.[14] The average sputtered atom energy is dependent on the dc sputtering voltage, given by $E = U_s \ln(\gamma E_{ion}/U_s) - U_s$, where $U_s$ is the surface energy barrier for the atoms to escape from the target, $\gamma = (4M_1M_2)/(M_1 + M_2)^2$ with $M_1$ and $M_1$ being the incident and sputtered particle weight, respectively, and $E_{ion}$ is the incident Ar ion energy (proportional to the sputtering voltage). This equation gives sputtered Co atom energy at 4.85 eV and 6.3 eV under sputtering voltage of 400 V and 600 V, respectively. Similar conclusion could be drawn about the fast neutrals, which are back-reflected Ar ions combined with electrons. These energetic particles, especially the high-energy fast neutrals, bombard the sample surface and improve the diffusivity of the adatoms, leading to enhanced film homogeneity and lower surface roughness.[15] Fig. 2 demonstrates the reduction of coercivity with increasing sputtering voltage, noticeably with CZT showing a monotonic trend.

After determining the individual FM layer thickness and the deposition conditions, we examine the shape anisotropy and the interaction between the FM layers in elongated, multilayer structures. For applications in integrated inductors, lateral dimensions of several hundred microns are of the most interest.[4] One of our potential implementations of the magnetic core structures is described in Ref. 16. We investigate FM/$SiO_2$($t_{SiO_2}$ nm)/FM trilayers with the optimized FM layer thickness. The $SiO_2$ layer thicknesses are 4, 6, 10, 20 and 40 to explore the coupling effects between the FM layers. The films are patterned using photolithography and liftoff process, into stripes (1 cm × 150 $\mu$m) and rectangles (400 $\mu$m × 100 $\mu$m), with the induced EA parallel to the short axis of the patterned elements. The classic work of Slonczewski[7] examined the domain configurations in infinitely long FM/NM/FM stripes thoroughly, and demonstrated the flux-closure between the two FM layers, leading to single-domain easy-axis state in the individual FM layer. The antiparallel alignment of magnetization in the two FM layers along the short axis in elongated FM/NM/FM sandwich structures could be inferred from the specific shape of the BH loop measured along the short axis, with a plateau at low applied field, centered at zero.[17] This feature is observed in all the CZT samples we explored for various $t_{SiO_2}$ (hysteresis loops not shown). We demonstrate in Fig. 3 the hysteresis loops for CZT(200 nm)/$SiO_2$(4 nm)/CZT(200 nm) stripes and rectangles. Note, however, that the plateau is much more

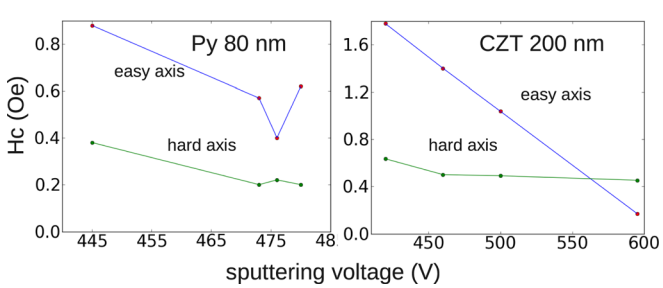


FIG. 2. Sputtering voltage dependence of coercivity ($H_c$) in uniaxial anisotropy extended single-layer films with the optimized thickness, Py 80 nm (left) and CZT 200 nm (right).

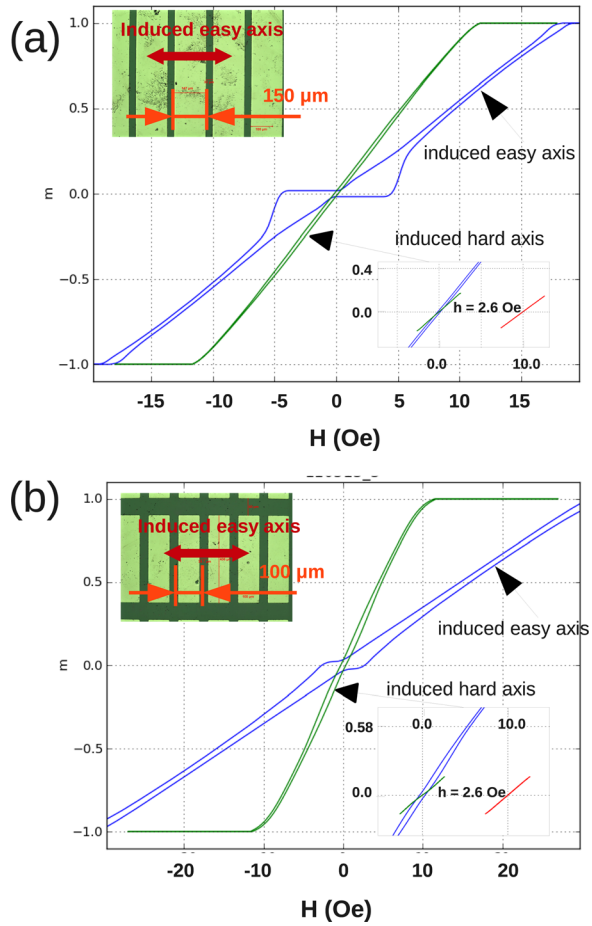


FIG. 3. BH loops for $Co_{91.5}Zr_{4.0}Ta_{4.5}(200\,nm)/SiO_2(4\,nm)/Co_{91.5}Zr_{4.0}Ta_{4.5}(200\,nm)$ structures. The inset at the lower right minor loops on induced hard axis showing linear response with negligible hysteresis loss, at 0 and 10 Oe bias fields. The permeability is slightly reduced in minor loops. (a) 1 cm × 150 $\mu$m and (b) 400 $\mu$m × 100 $\mu$m.

accentuated in the long stripes (Fig. 3(a)) than in the rectangles (Fig. 3(b)). A possible explanation for the weakening of this antiparallel flux-closure between the FM layers is the extra demagnetizing effect introduced by the sharp corners of the rectangular shape, preventing the local formation of edge curling wall.[7] In the theoretical models of Slonczewski, the FM/NM/FM stripes are infinitely long, and the effects at the ends are eliminated. In our case, the stripes 1 cm × 150 $\mu$m are better suited to the theoretical model.

Furthermore, we did not observe any plateau in the $Py(80\,nm)/SiO_2(t_{SiO_2}\,nm)/Py(80\,nm)$ systems (loops not shown). An estimation of the shape anisotropy in the Py elements, $H_{shape} = M_s(2t/\pi)(1/w - 1/l)$, where t is the thickness, w is the width, and l is the length of the FM slab, respectively, gives 4.5 Oe, which is at least equivalent to, if not dominating over the induced anisotropy $H_k = 3.5$ Oe. A further investigation on the domain configuration in a rectangular (30 $\mu$m × 7.5 $\mu$m) heterostructure $Ni_{80}Fe_{20}(23\,nm)/Ta(4\,nm)/Co_{40}Fe_{40}B_{20}(15\,nm)$ was carried out using scanning transmission x-ray microscopy at the Canadian Light Source SM beamline. Fig. 4 demonstrates the alignment of domains in the induced easy axis in the CoFeB element (having similar $4\pi M_s$ and $H_k$ to CZT), while the Py element forms classic diamond structures.

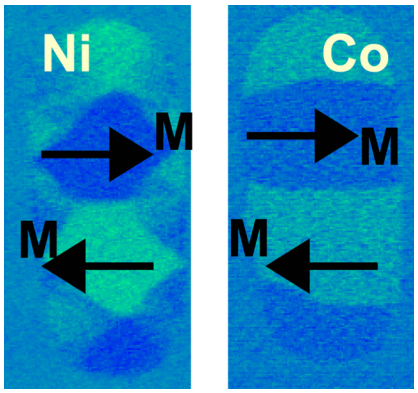


FIG. 4. Domain imaging using STXM, with the x-ray photon energy set to Ni $L_3$ edge for the top Py layer (left panel, showing diamond structure) and Co $L_3$ edge for the bottom CoFeB layer (right panel, magnetization along the induced easy axis); the dark and bright contrasts refer to magnetization pointing to the right and left, respectively.

We have shown in this paper, together with our previous work,[6] the control of well-defined high-permeability axis in micron-patterned, multilayered structures. We demonstrated in the CZT system the ability to align the magnetization transverse to the long axis in finite elongated structures, with optimized 3d dimensions for the interest of integrated inductors, leading to extremely low hysteresis loss and high permeability along the net magnetic flux path. These structures make up the segments in a toroidal magnetic core. With rotating induced anisotropy in adjacent sandwich trilayers in a multilayered film (with tens of laminations), isotropic high-permeability flux-closed core could be achieved.

We acknowledge support from the US Department of Energy Grant No. DE-EE0002892 and National Science Foundation ECCS-0925829.

[1]J. M. Wright, D. W. Lee, A. Mohan, A. Papou, P. Smeys, and S. X. Wang, IEEE Trans. Magn. **46**, 2387 (2010).
[2]M. Frommberger, C. Schmutz, M. Tewes, J. McCord, W. Hartung, R. Losehand, and E. Quandt, IEEE Trans. Microwave Theory Tech. **53**, 2096 (2005).
[3]D. W. Lee, K. P. Hwang, and S. X. Wang, IEEE Trans. Magn. **44**, 4089 (2008).
[4]C. Mathuna, N. Wang, S. Kulkarni, and S. Roy, IEEE Trans. Power Electron. **27**, 4799 (2012).
[5]M. Frommberger, J. McCord, and E. Quandt, IEEE Trans. Magn. **40**, 2703 (2004).
[6]C. Cheng, N. Sturcken, K. Shepard, and W. E. Bailey, Rev. Sci. Instrum. **83**, 063903 (2012).
[7]J. C. Slonczewski, B. Petek, and B. E. Argyle, IEEE Trans. Magn. **24**, 2045 (1988).
[8]H. Clow, Nature **194**, 1035 (1962).
[9]Y. Shimada and N. Saito, Jpn. J. Appl. Phys., Part 1 **25**, 419 (1986).
[10]H. Kronmuller, J. Magn. Magn. Mater. **24**, 159 (1981).
[11]R. J. Spain and H. Rubinstein, J. Appl. Phys. **32**, 288S (1961).
[12]D. S. Gardner, G. Schrom, P. Hazucha, F. Paillet, T. Karnik, and S. Borkar, J. Appl. Phys. **103**, 07E927 (2008).
[13]A. Hubert and R. Schaefer, *Magnetic Domains: the analysis of magnetic microstructures* (Springer, Berlin, 1998).
[14]K. Hayashi, M. Hayakawa, Y. Ochiai, H. Matsuda, W. Ishikawa, Y. Iwasaki, and K. Aso, J. Appl. Phys. **61**, 2983 (1987).
[15]J. J. Quan, X. W. Zhou, and H. N. G. Wadley, Surf. Sci. **600**, 2275 (2006).
[16]N. Sturcken, R. Davies, C. Cheng, W. E. Bailey, and K. Shepard, in *IEEE Applied Power Electronics Conference and Exposition (APEC)* (2012), p. 417.
[17]U. Queitsch, J. McCord, A. Neudert, R. Schafer, L. Schultz, K. Rott, and H. Bruckl, J. Appl. Phys. **100**, 093911 (2006).